Structural Basis of the Drug-binding Specificity of Human Serum Albumin

Jamie Ghuman[1], Patricia A. Zunszain[1], Isabelle Petitpas[1] Ananyo A. Bhattacharya[1], Masaki Otagiri[2] and Stephen Curry[1]*

[1]*Biophysics Section, Division of Cell and Molecular Biology Imperial College London, South Kensington Campus, London SW7 2AZ, UK*

[2]*Faculty of Pharmaceutical Sciences, Kumamoto University 5-1 Oe-honmachi, Kumamoto 862-0973, Japan*

Human serum albumin (HSA) is an abundant plasma protein that binds a remarkably wide range of drugs, thereby restricting their free, active concentrations. The problem of overcoming the binding affinity of lead compounds for HSA represents a major challenge in drug development. Crystallographic analysis of 17 different complexes of HSA with a wide variety of drugs and small-molecule toxins reveals the precise architecture of the two primary drug-binding sites on the protein, identifying residues that are key determinants of binding specificity and illuminating the capacity of both pockets for flexible accommodation. Numerous secondary binding sites for drugs distributed across the protein have also been identified. The binding of fatty acids, the primary physiological ligand for the protein, is shown to alter the polarity and increase the volume of drug site 1. These results clarify the interpretation of accumulated drug binding data and provide a valuable template for design efforts to modulate the interaction with HSA.

*Corresponding author

Introduction

Problems associated with adsorption, distribution, metabolism and elimination (ADME) add considerably to the complexity and cost of the development of new drugs[1] and are driving the search for techniques to optimise ADME characteristics at an early stage in the design process. One of the most important factors affecting the distribution and the free, active concentration of many administered drugs is binding affinity for human serum albumin (HSA). Albumin, the most abundant protein in human plasma ($\sim$600 μM), is a 66 kDa monomer containing three homologous helical domains (I–III), each divided into A and B subdomains (Figure 1(a)). The protein binds a wide variety of endogenous ligands including non-esterified fatty acids, bilirubin, hemin and thyroxine,[2] all of them acidic, lipophilic compounds, in multiple sites.[3–8] Many commonly

used drugs with acidic or electronegative features (e.g. warfarin, diazepam, ibuprofen) also bind to HSA, usually at one of two primary sites (1 and 2), located in subdomains IIA and IIIA, respectively[9,10]. While a degree of albumin-binding may be desirable in helping to solubilize compounds that would otherwise aggregate and be poorly distributed, drugs with an excessively high affinity for the protein ($>$95% bound) require correspondingly higher doses to achieve the effective concentration *in vivo*, can be slow to distribute to sites of action and may not be efficiently eliminated.[11–14]

Structural information on HSA–drug interactions has emerged only very recently and in a rather piecemeal fashion,[10,15–17] so most studies of drug binding have therefore adopted a ligand-based approach to the problem. For example, marker ligands for sites 1 and 2 have commonly been used in competition assays to identify the locus of binding of a range of different compounds.[9,18–20] More recently several pharmaceutical companies have developed high-throughput methods to assay the albumin-binding properties of their compound libraries.[13,21–25] The accumulated data can be used to develop quantitative structure–activity relationships for albumin binding.[12,14,26,27] However, the interpretation of competition or binding data is
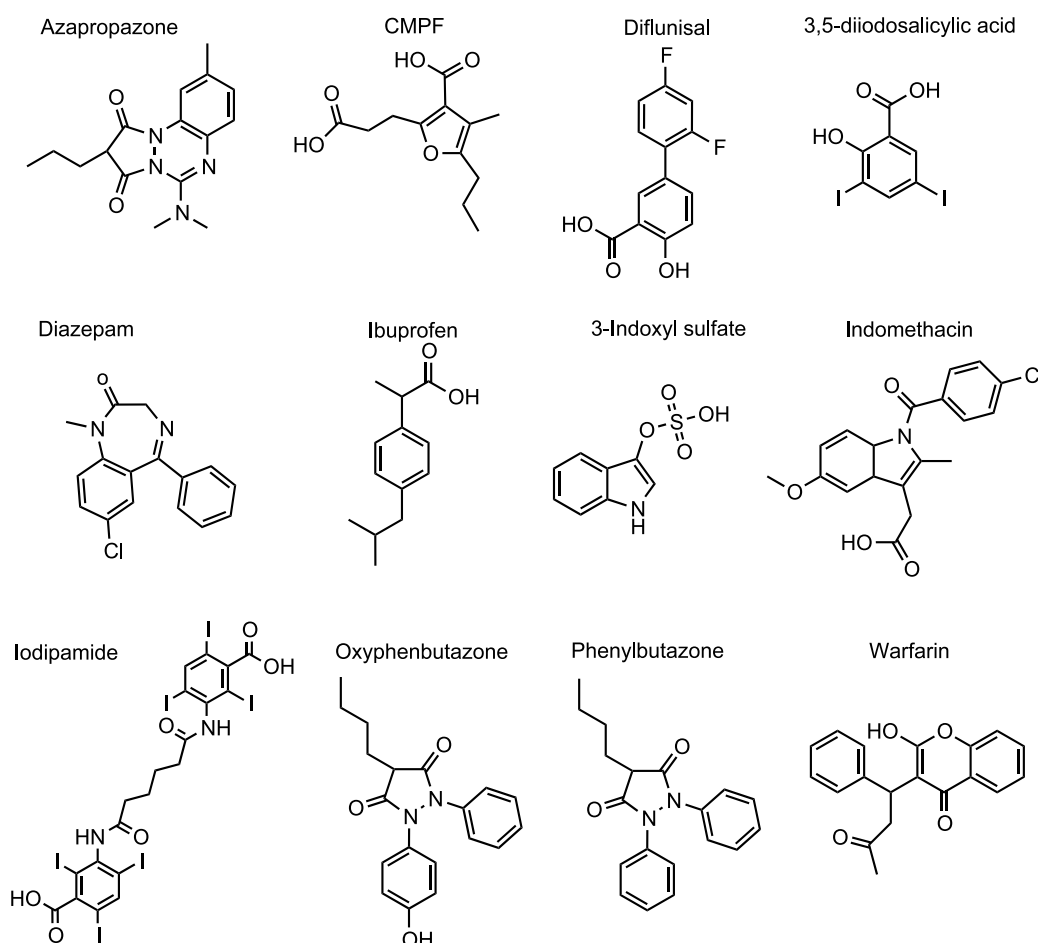
Figure 1. Chemical structures of the drug and toxin molecules used in this study.

non-trivial given the identification of partially overlapping binding compartments in site 1,[18–20] uncertainty as to the number of secondary drug-binding sites on the protein[20,28] and the possibility of allosteric interactions between drugs bound to sites 1 and 2.[29,30] Further complexities arise *in vivo* due to interactions between drugs and endogenous ligands for HSA.[31–33] This is particularly pertinent for fatty acids, which normally occur in serum at levels of between 0.1 and 2 mol per mol of HSA and can both compete and cooperate with drugs binding to the protein. In certain disease states, these effects are exacerbated as the fatty acid:HSA mole ratio may be as high as six.[34] Other pathological conditions are associated with high (micromolar to millimolar) levels of bilirubin, hemin or renal toxins (e.g. 3-carboxy-4-methyl-5-propyl-2-furanpropanoic acid (CMPF), indoxyl sulphate) which bind to the protein causing significant drug binding defects.[35–37]

Thus, although correlations based on large datasets of measurements of drug binding affinity have highlighted the importance of molecular descriptors such as lipophilicity, acidity, hydrogen bonding potential and shape factors in determining albumin binding,[13,27,38] such ligand-based approaches have yet to provide a wholly robust method for predicting the affinities of new compounds and structural information is clearly required to complement these investigations. We present here a crystallographic analysis of HSA complexed with a structurally diverse set of 12 drugs and small-molecule toxins (that are known to inhibit drug binding in renal patients), all of which bind to either site 1 or site 2[9,12,13,18,28,39,40] (Figure 1). We have also investigated the structural impact of drug–drug and drug–fatty acid interactions on the protein. The results provide new insights into the architecture and specificity of each drug pocket on HSA and reveal the molecular basis of the adaptability of this versatile transporter protein.

Results and Discussion

Structure determination and overview

HSA–drug and HSA-myristate–drug complexes were prepared either by co-crystallisation or crystal-soaking using relatively high (millimolar) drug concentrations, to help overcome the effect of the presence of ~30% (v/v) polyethlyene glycol in the crystal and thereby ensure good occupancy (Materials and Methods; Supplementary Data). The

structures of the drug complexes were solved by molecular replacement using previously determined structures of HSA[16] or HSA-myristate[4] as appropriate, since there were no gross conformational changes associated with drug binding. The shape of the difference electron density, coupled with consideration of the chemical nature of the binding environment, generally gave an unambiguous indication of the bound drug conformation (Figure 2). In a few cases, particularly complexes that were determined at lower resolutions (~3 Å), refinement of alternative drug orientations was used to determine the most plausible conformation. Models for the various complexes were refined to resolutions of 2.25–3.20 Å and have R_{free} values in the range 24.3–29.2% and good stereochemistry (Table 1).

Drug site 1 in defatted HSA

Drug site 1 is a pre-formed binding pocket within the core of subdomain IIA that comprises all six helices of the subdomain and a loop-helix feature (residues 148–154) contributed by IB. The interior of the pocket is predominantly apolar but contains two clusters of polar residues, an inner one towards the bottom of the pocket (Y150, H242, R257) and an outer cluster at the pocket entrance (K195, K199, R218, R222) (Figure 3). The large binding cavity is comprised of a central zone from which extend three distinct compartments. The back end of the pocket is divided by I264 into left and right hydrophobic sub-chambers (according to the viewpoint in Figure 3(a)–(c)), whereas a third sub-chamber protrudes from the front of the pocket, delineated by F211, W214, A215, L238 and aliphatic portions of K199 and R218.

As expected, CMPF, oxyphenbutazone, phenylbutazone and warfarin cluster in the centre of the site 1 pocket. In site 1 the ligands invariably have a planar group pinned snugly between the apolar side-chains of L238 and A291; in contrast there is much greater variation in the drug position within the plane perpendicular to the line between these two residues. This is particularly evident at the mouth of the pocket where the wide opening and
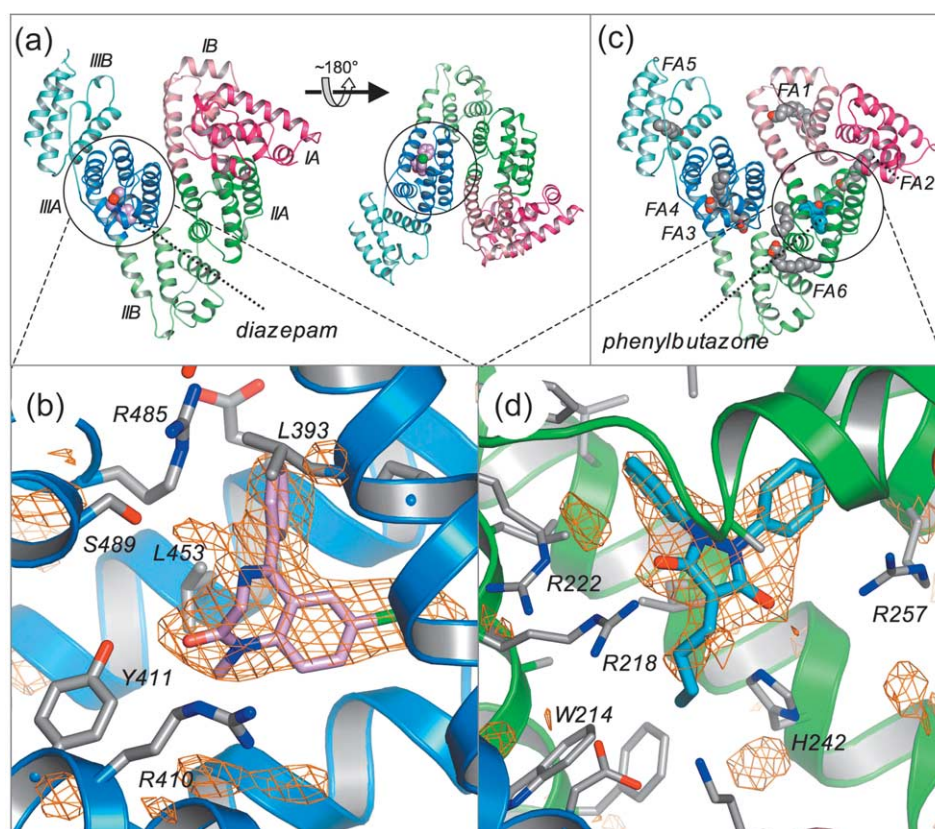
Figure 2. Overview of HSA structure and omit maps. (a) Structure of HSA–diazepam. The protein is colour-coded by subdomain using a scheme that is maintained throughout. The diazepam is depicted in space-filling representation colour-coded by atom-type: carbon, pink; oxygen, red; nitrogen, blue; chlorine, gr. The rotated view on the right shows drug site 2 in the same orientation as drug site 1 in (c). (b) F_o-F_c simulated annealing omit map calculated in CNS[50] with the diazepam molecule omitted from the phasing model and contoured at 2.75σ. (c) Structure of HSA-myristate-phenylbutazone. Fatty acid molecules and phenylbutazone are depicted in space-filling representation with carbon atoms coloured grey and mid-blue, respectively. (d) F_o-F_c simulated annealing omit map calculated with the phenylbutazone molecule omitted from the phasing model and contoured at 2.75σ. All Figures were prepared using PyMol.[55]

Table 1. Data collection and refinement statistics

Drug site	Myr[a]	Drug[b]	SG[c]	Resolution (Å)	N_{ref}[d]	R_{merge} (%)[e]	I/σ_I[f]	Multi-plicity	Complete-ness (%)	N_{atoms}[g]	R_{work} (%)	R_{free} (%)	B_{av} (Å²)	rms$_{bonds}$ (Å)	rms$_{angles}$ (Å)	PDB ID
1	−	aza	P1	41.4–2.70	32,322	4.1 (30.5)	12.2 (2.9)	2.0 (2.0)	95.6 (95.4)	8669	23.6	27.4	77.9	0.009	1.42	2bx8
1	−	cmpf	P1	49.2–2.35	50,096	3.6 (37.6)	10.3 (2.2)	1.8 (1.7)	95.5 (95.2)	8664	23.1	26.1	68.6	0.007	1.20	2bxa
1	−	oxy	P1	22.9–3.20	22,484	7.2 (34.2)	8.0 (2.5)	1.8 (1.8)	96.8 (97.0)	8790	22.8	27.6	71.0	0.006	1.23	2bxb
1	−	pbz	P1	36.4–3.10	22,396	10.5 (35.0)	7.0 (2.0)	2.0 (2.0)	98.4 (98.4)	8804	25.2	29.2	72.7	0.005	1.02	2bxc
1	−	wrf	P1	49.3–3.05	23,406	6.0 (36.9)	8.9 (2.3)	1.9 (1.9)	97.7 (97.0)	8632	21.3	26.0	73.2	0.008	1.29	2bxd
1	+	aza	C2	34.4–2.45	24,928	5.4 (38.1)	10.9 (3.2)	2.5 (2.5)	99.3 (99.9)	4633	20.8	26.5	54.5	0.007	1.21	2bxi
1	+	aza-imn	C2	22.3–2.40	25,123	4.1 (32.2)	13.6 (3.6)	2.6 (2.5)	95.1 (95.1)	4648	20.9	25.3	49.8	0.007	1.21	2bxk
1	+	dis	C2	12.8–2.60	17,736	5.2 (19.8)	12.4 (4.4)	2.4 (2.3)	83.9 (87.2)	4565	20.0	24.3	59.9	0.007	1.21	2bxl
1	+	imn	C2	34.5–2.5	23,052	5.7 (38.7)	8.4 (2.1)	1.7 (1.7)	97.8 (97.8)	4665	20.1	24.8	57.5	0.007	1.24	2bxm
1	+	iod	C2	34.5–2.65	19,370	5.4 (37.6)	11.4 (3.0)	2.7 (2.7)	97.8 (99.6)	4671	20.8	26.5	56.7	0.007	1.26	2bxn
1	+	oxy	C2	38.0–2.60	20,377	6.0 (40.0)	10.9 (2.9)	2.9 (2.9)	96.9 (98.4)	4648	19.5	25.3	58.8	0.007	1.26	2bxo
1	+	pbz	C2	34.4–2.30	28,916	6.1 (31.1)	10.0 (2.7)	2.1 (2.1)	96.8 (97.8)	4651	21.1	25.0	51.3	0.006	1.18	2bxp
1	+	pbz-imn	C2	22.3–2.60	20,764	5.4 (36.3)	13.1 (3.5)	3.0 (3.0)	98.6 (99.4)	4658	19.5	25.7	52.0	0.007	1.24	2bxq
2	−	dfl	P1	38.2–2.95	26,848	5.0 (32.5)	9.4 (2.4)	2.0 (2.0)	98.4 (98.2)	8710	22.6	27.0	82.0	0.009	1.32	2bxe
2	−	dzp	P1	22.6–2.90	27,722	4.8 (36.1)	10.8 (2.6)	1.9 (1.9)	96.6 (96.8)	8615	21.5	26.2	81.5	0.007	1.25	2bxf
2	−	ibu	P1	22.4–2.70	33,880	4.6 (32.1)	11.2 (2.8)	2.0 (1.9)	96.8 (96.6)	8773	23.4	28.2	75.0	0.007	1.22	2bxg
2	−	ids	P1	36.3–2.25	58,748	3.9 (38.6)	10.7 (2.5)	2.0 (2.0)	98.7 (98.1)	8625	22.7	26.6	69.3	0.009	1.32	2bxh

[a] Indicates presence or absence of myristate in the HSA–drug complex.
[b] Abbreviated names for drugs used here and in Figures are: aza, azapropazone; cmpf, 3-carboxy-4-methyl-5-propyl-2-furanpropanoic acid; dfl, diflunisal; dis, diiodosalicylic acid; dzp, diazepam; ibu, ibuprofen; ids, indoxyl sulfate; imn, indomethacin; iod, iodipamide; oxy, oxyphenbutazone; pbz, phenylbutazone; rwf, $R(+)$-warfarin.
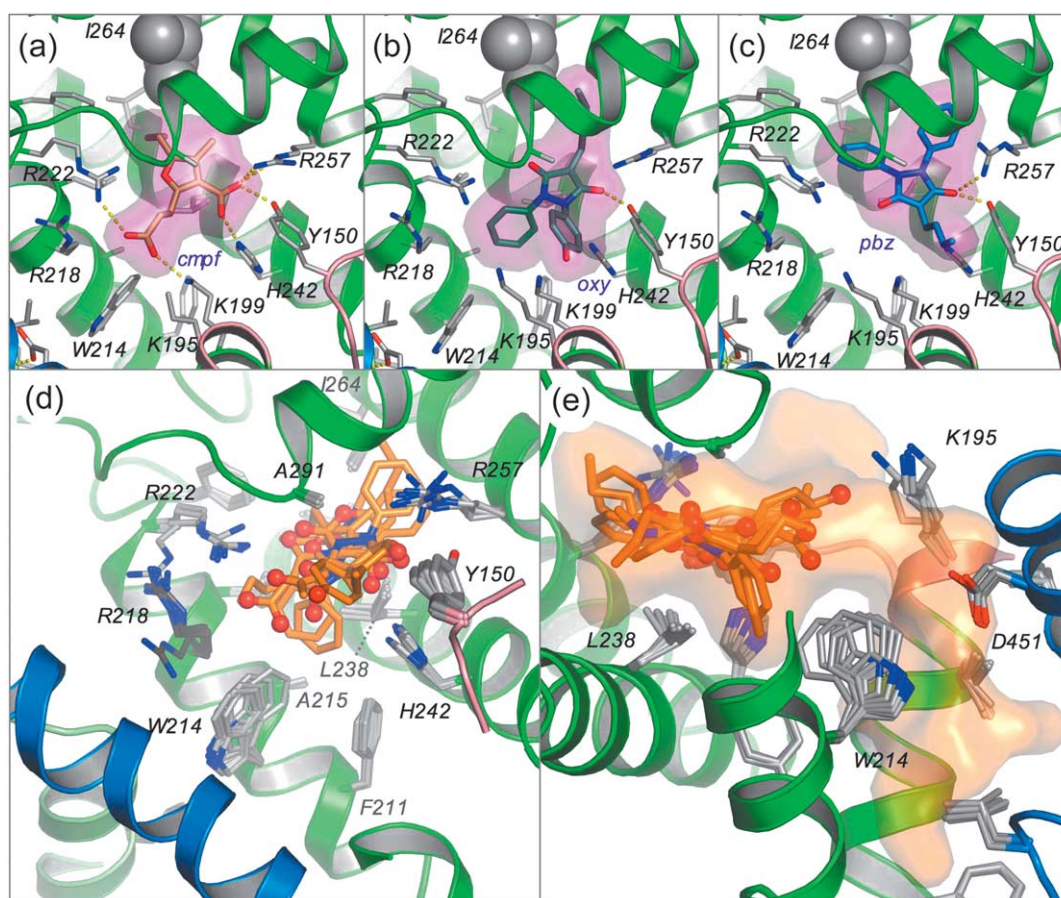[c] Space group.
[d] Number of independent reflections.
[e] Figures in parentheses indicate values for highest-resolution shell.
[f] Signal to noise ratio output from SCALA.
[g] Total number of atoms in the refined model.

Figure 3. Drug binding to site 1 in HSA (defatted). The detailed binding conformations are shown for (a) CMPF, (b) oxyphenbutazone and (c) phenylbutazone. In each case the drug is shown in a stick representation with a semi-transparent van der Waals surface. Abbreviated names for drugs are defined in the footnotes to Table 1. Selected side-chains are shown as sticks colour-coded by atom type; yellow dashed lines indicate hydrogen bonds. Residue I264, which bifurcates the back-end of the pocket, is shown as grey spheres. Note that the tip of K195 is disordered in the HSA–CMPF complex so the side-chain amino group is not shown in (a). (d) Top view of the superposition of drugs bound to site 1 in defatted HSA. Drugs are shown in a stick representation with carbon atoms coloured orange, nitrogen atoms in blue and oxygen atoms (also shown as small spheres) in red. Oxygen atoms tend to cluster on either side of the binding pocket. (e) Side view of superposition of drugs shown in (d) along with a semi-transparent surface (orange) depicting the extent of the pocket as determined by combining the pseudo-atom output from PASS,[56] which maps potential pockets on the protein surface, with the superposed drugs bound to the pocket, to account for observed variation in pocket dimensions due to ligand binding.

presence of flexible side-chains provides significant room for manoeuvre.

The drugs occupy the apolar compartments of site 1 to different extents. All compounds access the right-hand sub-chamber to a greater (oxyphenbutazone, phenylbutazone, warfarin) or lesser (CMPF, thyroxine[6]) degree but only phenylbutazone and CMPF project hydrophobic moieties into the left-hand sub-chamber (Figure 3(a)–(c); Supplementary Figure 1). The front, lower sub-chamber is occupied by phenyl groups of oxyphenbutazone and warfarin, and one of the iodine atoms projecting from the outer phenyl ring of thyroxine.[6]

In addition to hydrophobic contacts the site 1 compounds make a number of specific interactions with residues belonging to the inner and outer polar clusters. All of the compounds are positioned to make a hydrogen bond interaction with the hydroxyl group of Y150, as found previously for thyroxine,[6] and this residue therefore assumes a central role in drug interactions. In total CMPF makes five hydrogen-bond or salt-bridge interactions with Y150, H242, K199 and R222 and appears particularly well adapted to the pocket (Figure 3(a)), an observation that probably explains the high-affinity binding of this compound ($K_d = 0.1$ μM),[41] despite its relatively polar nature.[12] Clearly the drug binding defect observed *in vivo* as CMPF levels rise in kidney patients[35,41] is due to specific steric blocking of drug site 1 by this compound. The *R*-(+) and *S*-(−) enantiomers of warfarin bind in essentially the same position as one another and appear capable of making a total of three hydrogen bonds with the residues that interact with CMPF (the acetonyl oxygen atom being able to bond alternately to K199 or R222;

Supplementary Figure 1(e)); the similarity of the binding environments for the enantiomers helps to explain the poor stereoselectivity of HSA for this drug.[42] Oxyphenbutazone and phenylbutazone both make just a single hydrogen bond interaction with Y150 in drug site 1 (Figure 3(b) and (c)). In each case an oxygen atom on the opposite side of the drug lies 4–6 Å from R222 and/or K199; it is possible that water molecules may bridge interactions with these residues but these are not evident at the present resolution of these structures (Table 1). Strikingly, although oxyphenbutazone is a derivative of phenylbutazone, possessing an additional hydroxyl group on one of the phenyl rings, it binds in a conformation that is rotated by about 180° with respect to phenylbutazone and places the hydroxyl group at the mouth of the pocket where it can interact with bulk solvent. This is a revealing example of the unpredictable effects that even minor structural modifications can have on drug binding.

The prevalence of basic residues and the absence of acidic ones define the specificity of the pocket. The observation that reagents that are specific for site 1 generally possess centrally located anionic or electronegative features[2,9,28] is due to location of polar patches in the middle of the pocket flanked by apolar regions. In fact the structural data suggest a refinement of this view in that the pocket appears to be specific for molecules with two anionic or electronegative features on opposite sides of the ligand that can simultaneously interact with the two polar patches (Figure 3(d)). The distance between these basic patches accounts for the finding that the presence of two electronegative groups separated by five to six bonds, as in CMPF, is particularly important for tight binding to site 1.[12,27]

Superposition of the HSA–drug complexes for site 1 compounds reveals that there are only small side-chain movements associated with drug binding, in contrast to the displacements observed in the complex with thyroxine, a significantly larger molecule (M_r 777 Da)[6] (Figure 3(d) and (e)). For CMPF and the drugs used in this study ($M_r \sim 310$ Da) the greatest movement is observed for Y150 and W214. Side-chain variability with this set of molecules seems rather modest given the scope provided by numerous aliphatic residues lining the pocket. It may be that the apparent adaptability of the pocket is more a product of its size, which does not place tight steric constrains on the binding of small drugs and allows co-binding of water molecules that can flexibly mediate interactions with the protein.

Drug site 1 in HSA-myristate

Upon binding of fatty acids, Y150 from
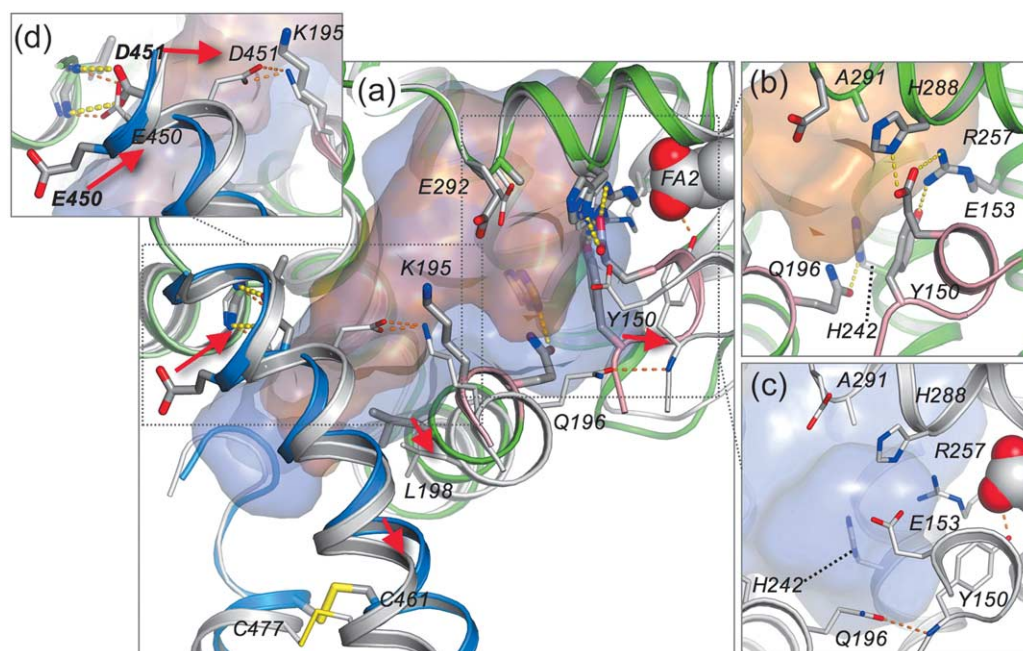
Figure 4. Conformational changes in drug site 1 as a result of fatty acid binding. (a) Superposition of HSA (secondary structure colour-coded by subdomain; selected side-chains coloured by atom type) and HSA-myristate (light-grey secondary structure with light grey carbon atoms in side-chains). Drug site 1 in HSA is depicted by a light-brown semi-transparent surface; binding of fatty acid results in expansion of drug site 1 (blue semi-transparent surface) as a result of concerted movement of several structural components. Red arrows indicate the direction of structural changes associated with fatty acid binding. (b) Close-up views of the region around Tyr150 in HSA and (c) HSA-myristate, colour-coded as in (a). (d) Rotated view of the vicinity of Glu450 and Asp451, which both rotate to new positions on fatty acid binding: Glu450 supplants Asp451 in interacting with the main-chain amides of residues 343–344 while Asp451 itself moves to form a salt-bridge with Lys195. Initial residue positions are labelled in boldface.

subdomain IB moves to interact with the carboxylate moiety of the lipid bound to the site that straddles domains I and II (fatty acid site FA2[3]) (Figure 4(a)–(c)). This helps to drive the relative rotation of domains I and II and has a large impact on one side of drug site 1 (Figure 2(a) and (c)). There is an extensive rearrangement of the H-bond network involving Y150, E153, Q196, H242, R257 and H288, which opens a solvent channel (between Y150 and Q196), thus increasing the volume of the pocket and altering its polarity distribution: the inner polar cluster is disrupted and partially neutralised by fatty acid binding; only H242 is relatively unaffected (Figure 4(b) and (c)). The helix containing L198 is also displaced outwards. This appears to impact an adjacent helix from subdomain IIIA (residues 442–466) and its disulphide-bonded neighbour. This latter helix is also twisted around its axis, since binding of myristate to site FA3 in IIIA replaces E450 in a salt-bridge interaction

with R348. As a result E450 rotates to replace D451 in interacting with the amide groups of residues 343–344 (Figure 4(d)). In turn, D451 relocates to a position that allows it to form a salt-bridge with K195. This cascade of interactions indicates one possible link between the two drug sites, at least in the presence of fatty acid.

To assess the impact of fatty acid-induced conformational changes on drug binding, we investigated the structure of HSA-myristate complexed with a range of site 1 drugs. The results are applicable to more physiologically relevant fatty acids, such as palmitate or oleate, since these exert the same conformational effects on the protein.[4,5] Although drug site 1 is co-incident with a fatty acid binding site (FA7),[4] this is likely to be a low-affinity site and in each case the drug was observed to displace the lipid.

In spite of the structural changes wrought by fatty acid binding, many of the features that emerged
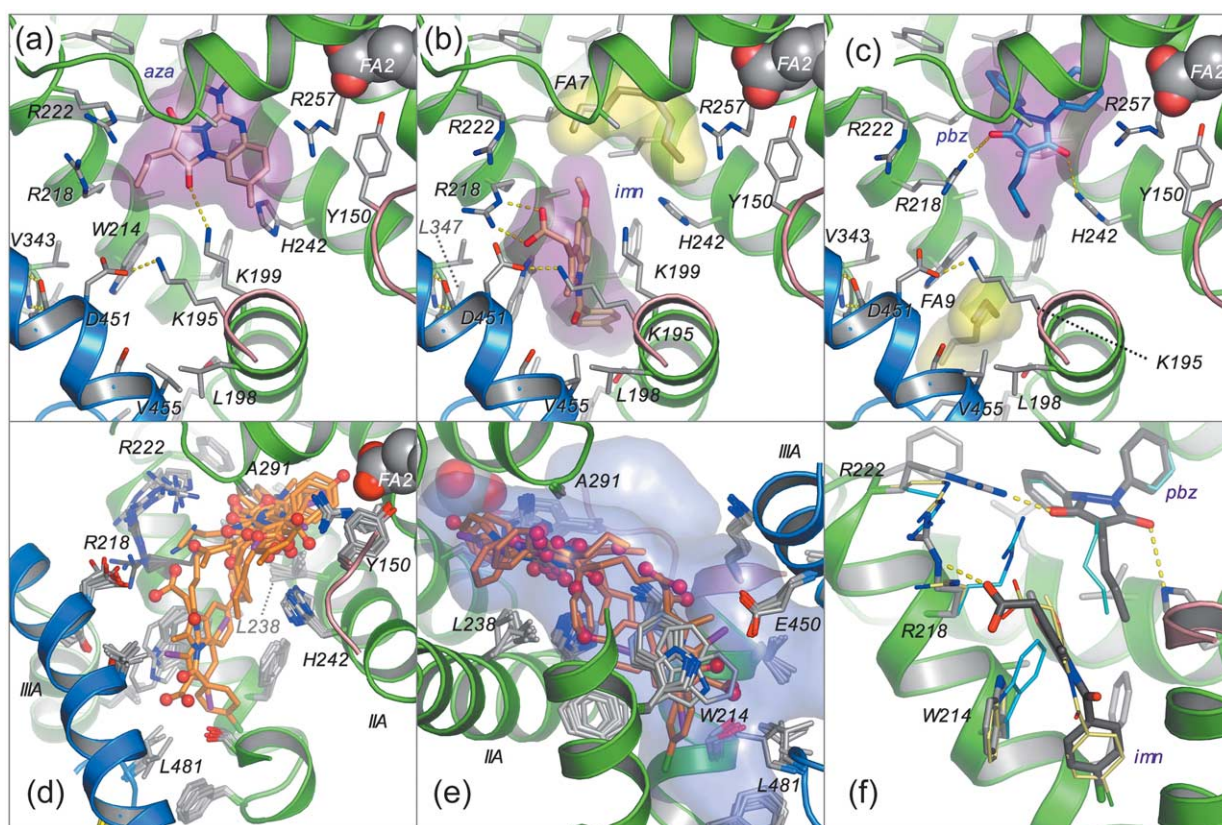
Figure 5. Drug binding to site 1 in HSA-myristate. The detailed binding conformations are shown for (a) azapropazone, (b) indomethacin and (c) phenylbutazone. In each case the drug is shown in a stick representation with a semi-transparent van der Waals surface (magenta). Bound fatty acids are depicted with a yellow semi-transparent van der Waals surface; otherwise colour-coding is as in Figure 3. The methylene tail of a molecule of myristate was observed co-bound with phenylbutazone in site FA9; this corresponds to a weak fatty acid site observed previously for medium-chain fatty acids.[4] (d) Top view of the superposition of drugs bound to site 1 in HSA-myristate (coloured as in Figure 3). In this case the clustering of oxygen atoms is less pronounced. (e) Side view of superposition of drugs shown in (d) along with a semi-transparent surface (blue) depicting the extent of the pocket, determined as described in the legend to Figure 3. (f) Superposition of the structure of HSA-myristate–indomethacin–phenylbutazone (secondary structure coloured by domain with drugs and selected side-chains shown as sticks with grey carbon atoms) with HSA-myristate–indomethacin (drug and side-chains shown as thin sticks with cream carbon atoms) and HSA-myristate–phenylbutazone (blue carbon atoms in side-chains).

from the comparison of complexes of site 1 drugs with defatted HSA were also evident in the presence of myristate (Figure 5). For example, with the notable exception of indomethacin (Figure 5(b)), all the compounds studied were again found to bind in the central portion of the binding cavity, pinned between L238 and A291 (Figure 5(d) and (e)). As before there was considerable variability in the lateral positioning of drugs in the plane defined by this grouping, with different drugs occupying the pocket sub-chambers to different extents.

Nevertheless, some remarkable differences were also observed. Since Y150 is removed from the pocket to interact with fatty acid, it is no longer available to make the central contribution to drug binding that is observed in complexes with defatted HSA. Rather, different drugs make use of the various basic and polar ligands on both sides of the binding pocket. Most interactions are made with the side-chains of K199 and R222 on one side of the pocket and H242 on the other, though R218 and R257 both interact specifically with some compounds (e.g. indomaethcin, phenylbutazone; Figure 5(b) and (c)).

For oxyphenbutazone, phenylbutazone and warfarin we have solved the structures of their complexes with HSA in the absence and presence of fatty acid. Comparison of the structures reveals only minor adjustments of the binding conformations of phenylbutazone (Figures 3(c) and 5(c)) and warfarin (Supplementary Figures 1(e) and 2(h)), a surprising result given that both drugs lose a specific interaction with Y150 on fatty acid binding, although interactions with H242 are retained. Interactions with solvent, as observed for warfarin,[15] may also help to compensate for the loss of Y150. In the presence of fatty acid, phenylbutazone rotates to insert one of its two phenyl groups about 1.5 Å further into the hydrophobic sub-chamber at the back end of the pocket and position a carbonyl group within 3.4 Å of the guanidinium group of R218 (compare Figures 3(c) and 5(c)). Warfarin slides forward by 1 Å to accommodate the new position of R257. Addition of fatty acids to HSA reportedly increases the affinity of site 1 for warfarin[28,31,32] but it is difficult to extract a precise molecular explanation for this effect from the structural data alone. One interesting difference is that the electron density for the coumarin ring of the drug at the back end of the pocket is significantly stronger in the HSA-myristate complex, suggesting that this moiety is more stably associated with the pocket in the presence of fatty acid. A similar observation was made for the phenyl rings of phenylbutazone, which also bind deep in the pocket, and we therefore suggest that fatty acid binding should also enhance the affinity of phenylbutazone.

In contrast to phenylbutazone and warfarin, oxyphenbutazone undergoes a re-orientation of about 180° due to fatty acid binding so that in the HSA-myristate complex this drug binds in a conformation that corresponds closely to that found for phenylbutazone (compare Supplementary Figure 1(c) and (d) with Supplementary Figure 2(f) and (g)). Thus in the presence of fatty acids the addition of a hydroxyl group to a phenyl ring in phenylbutazone has a minimal effect on the binding orientation.

In their complexes with HSA-myristate, oxyphenbutazone and phenylbutazone occupy both the left-hand and right-hand sub-chambers with phenyl or phenolic moieties (the phenolic hydroxyl of oxyphenbutazone makes a hydrogen bond to the main chain carbonyl oxygen of R257). In the case of di-iodosalicylic acid (DIS), tri-iodobenzoic acid (TIB)[3] and iodipamide, two of the iodine atoms on each ring overlie the positions of the aromatic rings in phenylbutazone and oxyphenbutazone (Supplementary Figure 2). This consistent positioning of iodine-substituted rings appears to be dictated by the shape of the binding site, in particular by the location of I264, which bifurcates the back end of the pocket into the two apolar sub-chambers. In addition, like oxyphenbutazone and phenylbutazone, the carboxylate groups of DIS and TIB both make hydrogen bonds with the side-chain of H242, which appears to assume a more prominent role in drug interactions than in defatted HSA.

Indomethacin is unusual in that it binds exclusively to the front, lower sub-compartment of site 1 and does not displace the fatty acid that is weakly bound to the centre of subdomain IIA (Figure 5(b)). In fact this drug can only be accommodated by inducing rotation of the side-chain of W214 through $\sim 160°$. This provides access to an additional cavity within IIA at the very base of the interdomain cleft that is largely delineated by L198, F206, A210, F211, W214 from IIA and L481 from subdomain IIIA; W214 also contacts residues V343 and L347 from IIB, so that the integrity of this cavity depends on contributions from three subdomains (Figure 5(b)). The chlorobenzoyl moiety of indomethacin binds at the bottom of this cavity while the indole ring is stacked between the flipped tryptophan and the apolar stem of K199. The indomethacin carboxylate group appears to make a bidentate salt-bridge to Arg218 (~ 2.8 Å) but there is only weak density for this moiety and an alternative conformation in which the carboxylate group flips over to interact with K199 may also be possible.

This expanded lower sub-chamber is also accessed by the contrast agent iodipamide (Supplementary Figure 2(e)), which is long enough to span the distance to the central portion of the site 1 pocket. Notably, iodipamide gains access to the lower chamber by inducing a much more modest $\sim 20°$ χ_1 rotation of the W214 side-chain in the opposite direction to that induced by indomethacin, thereby placing the indole ring in a plane anti-parallel conformation (Supplementary Figure 2(d) and (e)).

Superposition of the HSA-myristate–indomethacin structure with those for other HSA-myristate–drug

complexes suggested that indomethacin would co-bind with some other site 1 compounds such as azapropazone, oxyphenbutazone, phenylbutazone, DIS and TIB. We tested this idea by performing azapropazone–phenylbutazone and azapropazone–indomethacin double-drug soaks with HSA-myristate crystals. In both cases, the resulting difference electron density maps indicated that indomethacin was binding in contact with the second drug. The occupancies refined to >80% for the two drugs in each complex, indicating that they were binding simultaneously to the pocket on HSA. This interpretation is supported by the finding that the two drugs are slightly shifted in the double drug soaks by comparison to their positions in the corresponding single drug soaks, presumably as a result of drug–drug contacts (Figure 5(f); Supplementary Figure 3). The most striking effect of co-binding of these two drugs is the concerted rearrangement of R218 and R222, the principal effect of which is to substitute R222 instead of R218 as a binding partner for the carbonyl group of phenylbutazone (Figure 5(f)).

The simultaneous accommodation of indomethacin and either azapropazone or phenylbutazone in drug site 1 of the crystal structure is supported by binding data, which show that these drugs do not displace one another from HSA (A. Annis, personal communication).[18] These results were obtained using defatted HSA, indicating that co-binding also happens in the absence of fatty acid as expected from modelling experiments (data not shown). In contrast, comparison of the crystal structures suggests that indomethacin will not co-bind with every other site 1 drug. For example, we would predict steric clashes between indomethacin and iodipamide or warfarin (Supplementary Figure 2); this is consistent with binding data showing that indomethacin competes with warfarin.[18]

Superposition of all the drugs that have been analysed in complex with HSA-myristate reveals that site 1 extends significantly beyond the core of subdomain IIA (Figure 5(d) and (e)). The larger dataset of structures also reveals additional side-chain alterations associated with ligand binding. The greatest side-chain movements are again seen for residues at the mouth of the pocket, especially W214, the gatekeeper to the expanded lower sub-chamber, and the basic residues that make specific interaction with many of the bound drugs (K199, R218 and R222). This flexibility clearly contributes to the adaptability of the binding pocket. Within the pocket, packing constraints seem to restrict the side-chain variability in the HSA-myristate complex. Interestingly, although fatty acid binding displaces Y150 and Q196, thus opening up a new solvent channel with access to the protein exterior, none of the drugs studied here appears to take advantage of this new feature. The structural change nevertheless suggests ways in which compounds might be designed to specifically recognise the fatty acid-bound form of HSA.

For several drugs, secondary binding sites out-side subdomain IIA were observed in the HSA-myristate complex. Azapropazone, indomethacin and warfarin all bind in subdomain IB. With the exception of azapropazone, which displaced the fatty acid from subdomain IB, these compounds bound, apparently co-operatively with the lipid, in contact with its methylene tail. Conceivably these interactions will be altered by the presence of fatty acids longer than myristate which are more prevalent *in vivo*.[43] Interestingly, evidence for weak secondary binding in subdomain IB by azapropazone and warfarin was also observed in the absence of fatty acid (data not shown). An alternative mode of co-operativity was found for oxyphenbutazone, which makes a hydrogen bond *via* its hydroxyl group to the carboxylate group of the fatty acid bound to subdomain IIIB (FA5). A secondary iodipamide site that accommodates only one half of the molecule was found within the interdomain cleft, in precisely the same locus as the thyroxine site identified in the HSA-myristate complex.[6]

Drug site 2

Drug site 2 is composed of all six helices of subdomain IIIA and is therefore topologically similar to site 1 (subdomain IIA). Although, like site 1, it also comprises a largely pre-formed hydrophobic cavity with distinct polar features, there are significant differences between the two drug pockets. Drug site 2 is smaller than site 1; the principal binding region corresponds to the central portion of the site 1 pocket and appears to possess just one sub-compartment, the rear right-hand hydrophobic sub-chamber, though in this case the sub-chamber is only accessed following ligand-induced side-chain movements (see below). To a large extent the left-hand sub-chamber is eliminated by the presence of Y411, which occurs in subdomain IIIA at the position corresponding to L219 in IIA (Figure 6(a)). A further difference arises because, although the two drug sites are in structurally similar subdomains, these are packed in different contexts with respect to the remainder of the protein. The entrance to drug site 1 is enclosed by subdomains IIB and IIIA; residues from these subdomains contribute to the formation of the front sub-chamber which binds indomethacin and accommodates portions of iodipamide, phenylbutazone and warfarin. However, the entrance to site 2 is not encumbered in this way: although IIIA is followed by IIIB, this subdomain is rotated further away from the drug site entrance (in comparison to drug site 1, domain II) and leaves the pocket entrance more exposed to solvent (Figure 2(a) and (c)).

In contrast to site 1, drug site 2 has a single main polar patch, located close to one side of the entrance of the binding pocket and centred on Tyr411 but also including R410, K414 and S489 (Figure 6(a)–(c)). Of these residues only R410 and K414 occur in equivalent positions to polar-patch
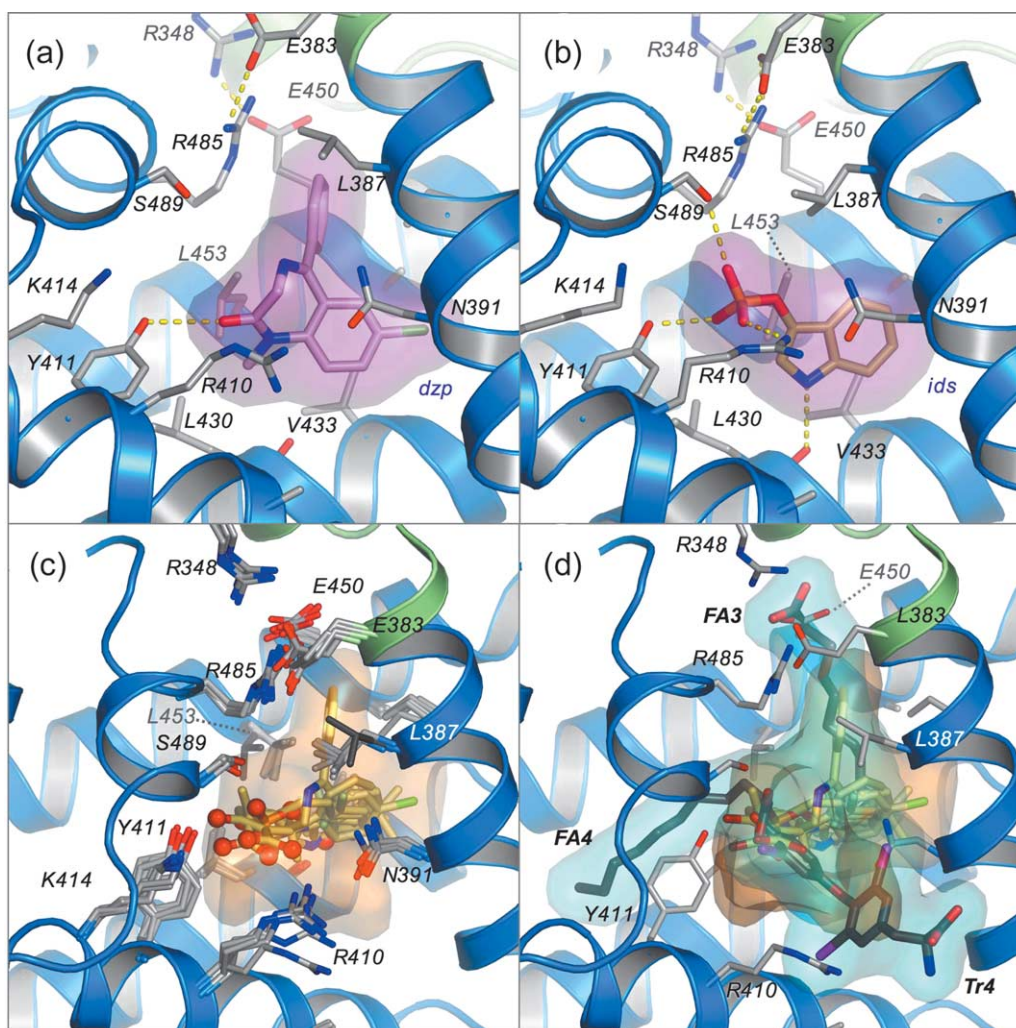
Figure 6. Drug binding to site 2 in HSA. The detailed binding conformations are shown for (a) diazepam and (b) indoxyl sulphate. In each case the drug is shown in a stick representation with a semi-transparent van der Waals surface (magenta). Colour-coding is as in Figure 3. (c) Top view of the superposition of drugs bound to site 2 in HSA along with a semi-transparent surface (orange) depicting the extent of the pocket. (d) Binding of endogenous ligands indicates possible expansion of drug site 2. Fatty acids (FA3 and FA4)[3,4] and thyroxine[6] which also bind to subdomain IIIA are added to the drug superposition shown in (c); the van der Waals surface defined for these endogenous ligands is coloured blue.

residues in drug site 1 (R218 and R222, respectively). Thus in terms of shape, size and polarity, drug sites 1 and 2 are clearly distinguishable and this helps to account for the different binding specificities of the two pockets.

Diflunisal, diazepam, ibuprofen and indoxyl sulphate all cluster in the centre of the binding pocket of subdomain IIIA, oriented with at least one oxygen atom in the vicinity of the polar patch (Figure 6(a)–(c); Supplementary Figure 4). In every case, there is an interaction with the hydroxyl group of Y410, whereas none of the drugs were found to interact with K414. R410 and S489 also contribute salt-bridge and hydrogen-bond interactions to drug binding, though not in the case of diazepam. Thus the observation that site 2 is generally selective for drugs with a peripherally located electronegative group[2] can be ascribed to the presence of a basic

polar patch located at one end of a generally apolar pocket in subdomain IIIA.

However, the uniform binding orientation of diflunisal, diazepam, ibuprofen and indoxyl sulphate contrasts with that of di-isopropyl phenol (propofol), a general anaesthetic drug. Due to steric effects of the isopropyl groups, the single polar hydroxyl group in the centre of the propofol molecule cannot interact with the main polar patch in drug site 2 and instead, propofol adopts a conformation that allows formation of a hydrogen bond to the carbonyl oxygen of Leu430.[16] Interestingly this carbonyl group also interacts with the indole amide of indoxyl sulphate and the bromine atom of halothane[16] and appears to constitute a secondary polar feature in the pocket (Supplementary Figure 4(d) and (g)).

There is comparatively little side-chain

movement associated with ligand binding if one considers just the smallest drugs (diflunisal, ibuprofen, halothane, indoxyl sulphate, and propofol; M_r 197–250 Da); V433 and R410 are the most susceptible to ligand-induced alterations (Figure 6(c)). However, binding of diazepam, which has a larger, branched structure (M_r 284.7 Da) is accompanied by large rotations of the side-chains of L387 and L453 that increases their separation from 5.4 Å to 7.7 Å and allows the phenyl ring of the drug to access the rear right-hand sub-chamber of the pocket. This pocket is closed off by R348-E450 and R485-E383 salt-bridges (Figure 6(c)). As in site 1, variations in the water structure, which was generally not visible at the resolutions of our structure determinations, may help to make the pocket more adaptable.

Further evidence of the adaptability of drug site 2 in subdomain IIIA derives from the fact that although it appears to be relatively small, it can bind two molecules of long-chain fatty acid (in fatty acid sites FA3 and FA4)[4] or one of thyroxine.[6] Comparison of drug and fatty acid binding reveals the very different ways in which these classes of ligand bind to a common locus on the protein (Figure 6(d)). In fact, drug site 2 is composed of the apolar region that is occupied by the methylene tails of fatty acids bound to FA3 and the polar patch that interacts with the carboxylate moiety of fatty acids bound to FA4. None of the drugs examined to date is observed to access the long, narrow hydrophobic tunnel of FA4 that accommodates the methylene tails of lipids bound to this site. Moreover, fatty acids bound to FA3 do not interact with the polar patch centred on Y411. Instead, binding of the fatty acid opens access to a different polar patch by inducing the same rotations of L387 and L453 that are observed upon diazepam binding and the lipid carboxylate group supplants E450 in a salt-bridge interaction with R348 in subdomain IIB (Figure 6(d)). These observations suggest possible ways in which drugs might be modified in order to take advantage of this flexible binding facility in the pocket.

Fatty acid binding is also known to be associated with a large conformational change in HSA, involving rotations of domains I and III relative to domain II, which suggests a possible molecular mechanism for allosteric interactions between fatty acid binding sites.[3,4,44] In contrast, the conformational changes observed for drug binding at sites 1 and 2 are more local; there is no evidence for the global conformational changes on the scale observed with fatty acid binding. The observed instances of allosteric interactions between drug sites 1 and 2[28–30] may possibly be due to more subtle structural effects or to the presence of additional binding sites.

Several of the site 2 compounds analysed also bind to additional sites outside subdomain IIIA.
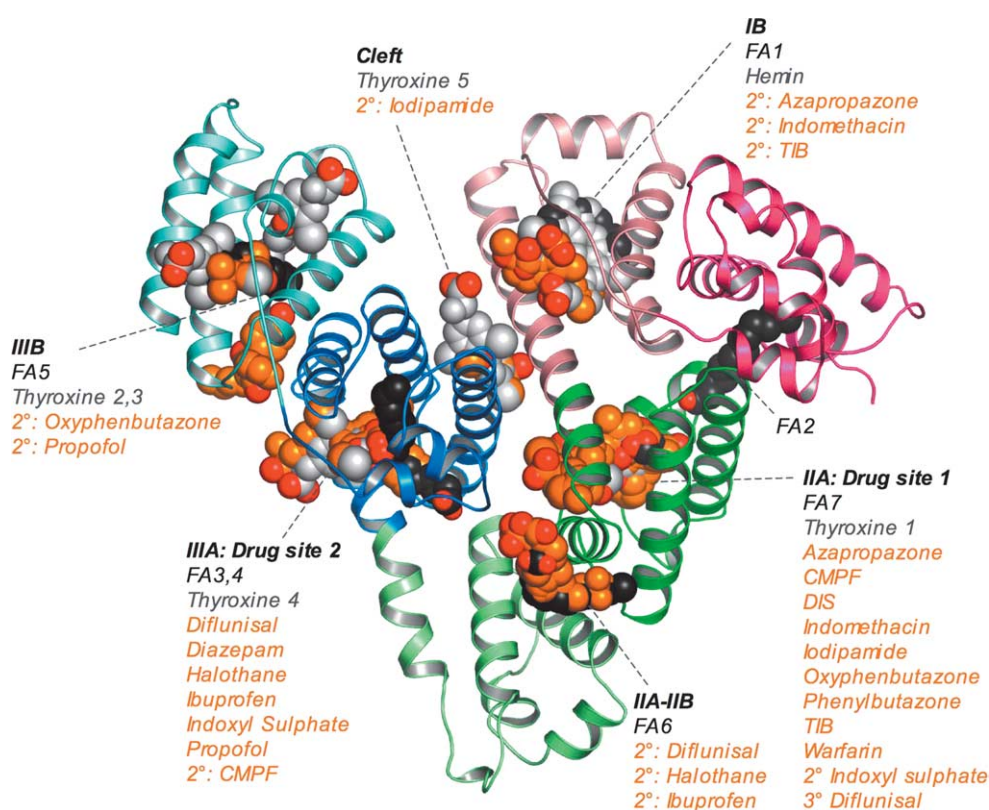
Figure 7. Summary of the ligand binding capacity of HSA as defined by crystallographic studies to date. Ligands are depicted in space-filling representation; oxygen atoms are coloured red; all other atoms in fatty acids (myristic acid), other endogenous ligands (hemin, thyroxin) and drugs are coloured dark-grey, light grey and orange, respectively.

A secondary binding site is observed for indoxyl sulphate in drug site 1 where two molecules of the compound appear to bind in overlapping and mutually exclusive conformations, one with the sulphate group positioned to interact with the inner polar patch and one in which the sulphate is salt-bridged to the outer patch at the pocket entrance. There is evidence to suggest that diflunisal and ibuprofen may also bind within site 1, though the density in the case of ibuprofen is rather weak and this drug was therefore not incorporated at this site in the refined model. In contrast the electron density maps clearly indicate that diflunisal and ibuprofen both occupy a previously undetected secondary site at the interface between subdomains IIA and IIB in a binding cleft that overlaps the fatty acid site FA6[4,5] (Figure 7). The carboxylate groups of the drugs interact with the side-chains of K351 and S480 (of subdomain IIIA) and the amide groups of L481 and V482. In this locus both drugs pack against the helix (residues 209–223) which forms part of the entrance to drug site 1; conceivably binding of diflunisal or ibuprofen to this secondary site may therefore impact the binding of site 1 drugs[28,29]. We did not observe a secondary site for diazepam.

Our structural data show that the two primary drug sites on HSA are highly adaptable binding cavities containing distinct sub-compartments, some of which are only accessed by local drug-induced conformational changes, and reveal a range of secondary binding sites distributed widely across the protein. In each case, the drug sites overlap with endogenous ligand-binding sites (Figure 7). The binding specificities of the pockets are determined by their shapes and the particular distributions of basic and polar residues on the largely hydrophobic interior walls that are involved in charge neutralization and hydrogen bonding interactions with acidic or electronegative small molecule ligands. The combination of shape-adaptability with specific polar interactions exhibited by HSA in these sites is reminiscent of the promiscuous binding site identified in QacR, a multi-drug binding protein from *Staphylococcus aureus*,[45] although, in contrast to HSA, QacR has a preference for cationic lipophilic drugs and its hydrophobic cavity is therefore studded with acidic glutamate side-chains. The detailed insights into HSA–drug interactions reported here provide an invaluable structural framework for the interpretation of drug binding data and will facilitate efforts to modify new therapeutic compounds to control their interaction with HSA and therefore optimise their distribution within the human body.

Materials and Methods

Protein purification, complex formation and crystallisation

Samples of purified recombinant HSA were kindly provided by Delta Biotechnology Ltd. (Nottingham, UK) and Professor Eishun Tsuchida (Waseda University, Japan). Prior to crystallisation in the absence of fatty acid, the protein was defatted[46] and subjected to gel-filtration to ensure a purely monomeric preparation.[3,16] Drugs were purchased as the highest purity preparations available from Sigma or Fluka. Azapropazone was kindly provided by Professor Ulrich Kragh-Hansen and CMPF was synthesised as described.[36] Crystals of defatted HSA generally do not tolerate soaking in ligand solutions so HSA–drug complexes were prepared before crystallisation by incubating the protein with a fivefold molar excess of drug at room temperature for 1–16 h. For example, 400 μl of HSA at 100 mg/ml (1.5 mM) was mixed with 600 μl of drug at 5 mM in 50 mM sodium phosphate buffer (pH 7). Where drug stock solutions were prepared in methanol or dimethyl sulphoxide, the maximum concentration of organic solvent at this stage was 7% (v/v). The free drug concentration was then fixed by repeated cycles of concentration and dilution in buffer containing 0.1 mM drug using a 10 kDa ultracentrifugation device (Millipore) and the protein concentration restored to 100 mg/ml; during this process any organic solvent present was reduced in concentration to less than 0.1% (v/v).

All crystals were grown by sitting-drop vapour diffusion using protein concentrations of around 100 mg/ml in 50 mM potassium phosphate (pH 7)[4,16,47]. The HSA–drug complexes were crystallised typically by mixing 2.5 μl of protein with 2.5 μl of a reservoir solution containing 24–30% (w/v) polyethylene glycol 3350 (Sigma-Aldrich), 50 mM potassium phosphate (pH 7.0).

HSA-myristate complexes were prepared (without prior defatting of the protein) and crystallised as described.[3,4] In all cases the largest crystals were obtained by streak- or micro-seeding into drops that had been allowed to equilibrate for 5–7 days.[48] Crystals were harvested into solutions containing slightly higher PEG 3350 concentrations than were used for crystallisation.[4] In a deviation from our previous practice, myristate was omitted from the harvest buffer in order to favour drug displacement of the fatty acid. Ternary HSA-myristate–drug complexes were prepared by soaking crystals of HSA-myristate in a series of harvest buffer solutions containing increasing concentrations of the requisite drug; typically the starting concentration was 0.1 mM and this was doubled every few minutes or hours up to the maximum tolerable concentration (~5 mM) (as judged by the fragmentation of crystals). Total soak times ranged from 2–48 h.

Data collection and structure determination

X-ray diffraction data were collected at room temperature using synchrotron radiation on station 9.6 at Daresbury SRS (UK) and stations BW7A, X11 and X13 at EMBL/DESY Hamburg (Germany) (Table 1). The data were indexed and measured with MOSFLM.[49] In all cases the HSA–drug complexes crystallised isomorphously with the P1 crystals of defatted HSA obtained previously in this laboratory.[16] The protein model for this structure (PDB ID, 1e78) was used as a starting model for phasing of the X-ray data. The model, split into its six subdomains, was first refined as a rigid body using CNS (version 1.1)[50] and then subjected to cycles of positional and B-factor refinement interleaved with manual model corrections in O.[51] Datasets for HSA-myristate–drug complexes were phased and refined in the same way using the original HSA-myristate structure (PDB ID 1e7g),[3,4] stripped of all its ligands, as the starting model.

Following initial refinement of the protein structure, difference electron density maps showed clear density for bound drug molecules and in each case defined the orientation and conformation of the bound ligand. Where possible, models for the drug molecules or their constituent fragments were obtained from the Cambridge Structural Database *via* the Chemical Database Service[52] and used to generate refinement dictionaries with XPLO2D.[53] In the case of CMPF, structure was generated using the Dundee PRODRG2 server.[54]

The HSA–drug complexes (with or without myristate) were refined to resolutions of 2.25–3.2 Å; the models have R_{free} values in the range 24.3–29.2% and good stereo-chemistry (Table 1). Average B-factors for the different models are relatively high, at around 55 Å^2 for HSA-myristate models ($C2$ space group) and 74 Å^2 for HSA without fatty acid ($P1$ space group). For both crystal forms, subdomain IIIB consistently exhibits higher than average B-factors, indicative of greater mobility of this region.

Protein Data Bank atomic coordinates

Atomic co-ordinates have been deposited with the RCSB Protein Data Bank (ID codes are given in Table 1).

Acknowledgements

Supplementary Data

Supplementary data associated with this article can be found at 10.1016/j.jmb.2005.07.075

References

1. Hodgson, J. (2001). ADMET—turning chemicals into drugs. *Nature Biotechnol.* **19**, 722–726.
2. Peters, T. (1995). *All About Albumin: Biochemistry, Genetics and Medical Applications*, Academic Press, San Diego.
3. Curry, S., Mandelkow, H., Brick, P. & Franks, N. (1998). Crystal structure of human serum albumin complexed with fatty acid reveals an asymmetric distribution of binding sites. *Nature Struct. Biol.* **5**, 827–835.
4. Bhattacharya, A. A., Grüne, T. & Curry, S. (2000). Crystallographic analysis reveals common modes of binding of medium and long-chain fatty acids to human serum albumin. *J. Mol. Biol.* **303**, 721–732.

5. Petitpas, I., Grüne, T., Bhattacharya, A. A. & Curry, S. (2001). Crystal structures of human serum albumin complexed with monounsaturated and polyunsaturated fatty acids. *J. Mol. Biol.* **314**, 955–960.
6. Petitpas, I., Petersen, C. E., Ha, C. E., Bhattacharya, A. A., Zunszain, P. A., Ghuman, J. *et al.* (2003). Structural basis of albumin–thyroxine interactions and familial dysalbuminemic hyperthyroxinemia. *Proc. Natl Acad. Sci. USA*, **100**, 6440–6445.
7. Zunszain, P. A., Ghuman, J., Komatsu, T., Tsuchida, E. & Curry, S. (2003). Crystal structural analysis of human serum albumin complexed with hemin and fatty acid. *BMC Struct. Biol.* **3**, 6.
8. Wardell, M., Wang, Z., Ho, J. X., Robert, J., Ruker, F., Ruble, J. & Carter, D. C. (2002). The atomic structure of human methemalbumin at 1.9 Å. *Biochem. Biophys. Res. Commun.* **291**, 813–819.
9. Sudlow, G., Birkett, D. J. & Wade, D. N. (1975). The characterization of two specific drug binding sites on human serum albumin. *Mol. Pharmacol.* **11**, 824–832.
10. He, X. M. & Carter, D. C. (1992). Atomic structure and chemistry of human serum albumin. *Nature*, **358**, 209–215.
11. Herve, F., Urien, S., Albengres, E., Duche, J. C. & Tillement, J. P. (1994). Drug binding in plasma. A summary of recent trends in the study of drug and hormone binding. *Clin. Pharmacokinet.* **26**, 44–58.
12. Kratochwil, N. A., Huber, W., Muller, F., Kansy, M. & Gerber, P. R. (2002). Predicting plasma protein binding of drugs: a new approach. *Biochem. Pharmacol.* **64**, 1355.
13. Valko, K., Nunhuck, S., Bevan, C., Abraham, M. H. & Reynolds, D. P. (2003). Fast gradient HPLC method to determine compounds binding to human serum albumin. Relationships with octanol/water and immobilized artificial membrane lipophilicity. *J. Pharm. Sci.* **92**, 2236–2248.
14. Colmenarejo, G. (2003). *In silico* prediction of drug-binding strengths to human serum albumin. *Med. Res. Rev.* **23**, 275–301.
15. Petitpas, I., Bhattacharya, A. A., Twine, S., East, M. & Curry, S. (2001). Crystal structure analysis of warfarin binding to human serum albumin: anatomy of drug site I. *J. Biol. Chem.* **276**, 22804–22809.
16. Bhattacharya, A. A., Curry, S. & Franks, N. P. (2000). Binding of the general anesthetics propofol and halothane to human serum albumin: high-resolution crystal structures. *J. Biol. Chem.* **275**, 38731–38738.
17. Mao, H., Hajduk, P. J., Craig, R., Bell, R., Borre, T. & Fesik, S. W. (2001). Rational design of diflunisal analogues with reduced affinity for human serum albumin. *J. Am. Chem. Soc.* **123**, 10429–10435.
18. Fehske, K. J., Schläfer, U., Wollert, U. & Müller, W. E. (1981). Characterization of an important drug binding area on human serum albumin including the high-affinity binding sites of warfarin and azapropazone. *Mol. Pharmacol.* **21**, 387–393.
19. Kragh-Hansen, U. (1988). Evidence for a large and flexible region of human serum albumin possessing high affinity binding sites for salicylate, warfarin and other ligands. *Mol. Pharmacol.* **34**, 160–171.
20. Yamasaki, K., Maruyama, T., Kragh-Hansen, U. & Otagiri, M. (1996). Characterization of site I on human serum albumin: concept about the structure of a drug binding site. *Biochim. Biophys. Acta*, **1295**, 147–157.
21. Hajduk, P. J., Mendoza, R., Petros, A. M., Huth, J. R., Bures, M., Fesik, S. W. & Martin, Y. C. (2003). Ligand

binding to domain-3 of human serum albumin: a chemometric analysis. *J. Comput. Aided Mol. Des.* **17**, 93–102.

22. Bertucci, C., Canepa, A., Ascoli, G. A., Guimaraes, L. F. & Felix, G. (1999). Site I on human albumin: differences in the binding of (*R*)- and (*S*)-warfarin. *Chirality,* **11**, 675–679.

23. Beaudry, F., Coutu, M. & Brown, N. K. (1999). Determination of drug-plasma protein binding using human serum albumin chromatographic column and multiple linear regression model. *Biomed. Chromatog.* **13**, 401–406.

24. Rich, R. L., Day, Y. S., Morton, T. A. & Myszka, D. G. (2001). High-resolution and high-throughput protocols for measuring drug/human serum albumin interactions using BIACORE. *Anal. Biochem.* **296**, 197–207.

25. Buchholz, L., Cai, C. H., Andress, L., Cleton, A., Brodfuehrer, J. & Cohen, L. (2002). Evaluation of the human serum albumin column as a discovery screening tool for plasma protein binding. *Eur. J. Pharm. Sci.* **15**, 209–215.

26. Colmenarejo, G., Alvarez-Pedraglio, A. & Lavandera, J. L. (2001). Cheminformatic models to predict binding affinities to human serum albumin. *J. Med. Chem.* **44**, 4370–4378.

27. Saiakhov, R. D., Stefan, L. R. & Klopman, G. (2000). Multiple computer-automated structure evaluation model of the plasma protein binding affinity of diverse drugs. *Perspectives Drug Disc. Des.* **19**, 133–155.

28. Sudlow, G., Birkett, D. J. & Wade, D. N. (1976). Further characterization of specific drug binding sites on human serum albumin. *Mol. Pharmacol.* **12**, 1052–1061.

29. Fitos, I., Visy, J., Simonyi, M. & Hermansson, J. (1999). Stereoselective allosteric binding interaction on human serum albumin between ibuprofen and lorazepam acetate. *Chirality,* **11**, 115–120.

30. Chen, J. & Hage, D. S. (2004). Quantitative analysis of allosteric drug-protein binding by biointeraction chromatography. *Nature Biotechnol.* **22**, 1445–1448.

31. Birkett, D. J., Myers, S. P. & Sudlow, G. (1977). Effects of fatty acids on two specific drug binding sites on human serum albumin. *Mol. Pharmacol.* **13**, 987–992.

32. Vorum, H. & Honoré, B. (1996). Influence of fatty acids on the binding of warfarin and phenprocoumon to human serum albumin with relation to anticoagulant therapy. *J. Pharm. Pharmacol.* **48**, 870–875.

33. Ivarsen, R. & Brodersen, R. (1989). Displacement of bilirubin from adult and newborn serum albumin by a drug and fatty acid. *Dev. Pharmacol. Ther.* **12**, 19–29.

34. Cistola, D. P. & Small, D. M. (1991). Fatty acid distribution in systems modeling the normal and diabetic human circulation. A ^{13}C nuclear magnetic resonance study. *J. Clin. Invest.* **87**, 1431–1441.

35. Henderson, S. J. & Lindup, W. E. (1990). Interaction of 3-carboxy-4-methyl-5-propyl-2-furanpropanoic acid, an inhibitor of plasma protein binding in uraemia, with human albumin. *Biochem. Pharmacol.* **40**, 2543–2548.

36. Tsutsumi, Y., Maruyama, T., Takadate, A., Goto, M., Matsunaga, H. & Otagiri, M. (1999). Interaction between two dicarboxylate endogenous substances, bilirubin and an uremic toxin, 3-carboxy-4-methyl-5-propyl-2-furanpropanoic acid, on human serum albumin. *Pharm. Res.* **16**, 916–923.

37. Sakai, T., Yamasaki, K., Sako, T., Kragh-Hansen, U., Suenaga, A. & Otagiri, M. (2001). Interaction

mechanism between indoxyl sulfate, a typical uremic toxin bound to site II, and ligands bound to site I of human serum albumin. *Pharm. Res.* **18**, 520–524.

38. Abraham, M. H., Ibrahim, A., Zissimos, A. M., Zhao, Y. H., Comer, J. & Reynolds, D. P. (2002). Application of hydrogen bonding calculations in property based drug design. *Drug Discov. Today,* **7**, 1056–1063.

39. Sjoholm, I., Ekman, B., Kober, A., Ljungstedt-Pahlman, I., Seiving, B. & Sjodin, T. (1979). Binding of drugs to human serum albumin: XI. The specificity of three binding sites as studied with albumin immobilized in microparticles. *Mol. Pharmacol.* **16**, 767–777.

40. Kragh-Hansen, U. (1985). Relations between high-affinity binding sites of markers for binding regions on human serum albumin. *Biochem. J.* **225**, 629–638.

41. Sakai, T., Takadate, A. & Otagiri, M. (1995). Characterization of binding site of uremic toxins on human serum albumin. *Biol. Pharm. Bull.* **18**, 1755–1761.

42. Loun, B. & Hage, D. S. (1994). Chiral separation mechanisms in protein-based HPLC columns. 1. Thermodynamic studies of (*R*)- and (*S*)-warfarin binding to immobilized human serum albumin. *Anal. Chem.* **66**, 3814–3822.

43. Saifer, A. & Goldman, L. (1961). The free fatty acids bound to human serum albumin. *J. Lipid Res.* **2**, 268–270.

44. Curry, S., Brick, P. & Franks, N. P. (1999). Fatty acid binding to human serum albumin: new insights from crystallographic studies. *Biochim. Biophys. Acta,* **1441**, 131–140.

45. Schumacher, M. A. & Brennan, R. G. (2003). Deciphering the molecular basis of multidrug recognition: crystal structures of the *Staphylococcus aureus* multi-drug binding transcription regulator QacR. *Res. Microbiol.* **154**, 69–77.

46. Sogami, M. & Foster, J. F. (1968). Isomerization reactions of charcoal-defatted bovine plasma albumin. The N–F transition and acid expansion. *Biochemistry,* **7**, 2172–2182.

47. Carter, D. C., Chang, B., Ho, J. X., Keeling, K. & Krishnasami, Z. (1994). Preliminary crystallographic studies of four crystal forms of serum albumin. *Eur. J. Biochem.* **226**, 1049–1052.

48. Stura, E. A. & Wilson, I. A. (1990). Analytical and production seeding techniques. *Methods,* **1**, 38–49.

49. Collaborative Computer Project No. 4. (1994). The CCP4 suite: programs for protein crystallography. *Acta Crystallog. sect. D,* **50**, 760–763.

50. Brünger, A. T., Adams, P. D., Clore, G. M., DeLano, W. L., Gros, P., Grosse-Kunstleve, R. W. *et al.* (1998). Crystallography & NMR system: a new software suite for macromolecular structure determination. *Acta Crystallog. sect. D,* **54**, 905–921.

51. Jones, T. A., Zou, J. Y., Cowan, S. W. & Kjeldgaard, M. (1991). Improved methods for building protein models in electron density maps and the location of errors in these maps. *Acta Crystallog. sect. A,* **47**, 110–119.

52. Fletcher, D. A., McMeeking, R. F. & Parkin, D. (1996). The United Kingdom Chemical Database Service. *J. Chem. Inf. Comput. Sci.* **36**, 746–749.

53. Kleywegt, G. J., Henrick, K., Dodson, E. J. & van Aalten, D. M. (2003). Pound-wise but penny-foolish: how well do micromolecules fare in macromolecular refinement? *Structure (Camb),* **11**, 1051–1059.

54. van Aalten, D. M., Bywater, R., Findlay, J. B., Hendlich, M., Hooft, R. W. & Vriend, G. (1996). PRODRG, a program for generating molecular

topologies and unique molecular descriptors from coordinates of small molecules. *J. Comput. Aided Mol. Des.* **10**, 255–262.

55. Delano, W. L. (2002). *The PyMOL Molecular Graphics System*, DeLano Scientific, San Carlos, CA, USA.

56. Brady, G. P. & Stouten, P. F. W. (2000). Fast prediction and visualization of protein binding pockets with PASS. *J. Comput. Aided Mol. Des.* **14**, 383–401.

Edited by R. Huber